RSC Advances

Photon assisted conducting atomic force microscopy study of nanostructured additives in P3HT:PCBM

Journal:	*RSC Advances*
Manuscript ID	RA-ART-09-2015-020266.R1
Article Type:	Paper
Date Submitted by the Author:	04-Nov-2015
Complete List of Authors:	Sahare, Sanjay; Defence Institute of Advanced Technology, Applied Physics Veldurthi, Naresh; Defence Institute of Advanced Technology, Applied Physics Datar, Suwarna; Department of Applied Physics, Defence Institute of Advanced Technology (DU),, Bhave, Tejashree; Defence Institute of Advanced Technology, Applied Physics
Subject area & keyword:	Materials < Physical

Journal Name

ARTICLE

Photon assisted conducting atomic force microscopy study of nanostructured additives in P3HT:PCBM

Received 00th January 20xx,
Accepted 00th January 20xx

DOI: 10.1039/x0xx00000x

www.rsc.org/

Sanjay Sahare, Naresh Veldurthi, Suwarna Datar[*b] and Tejashree Bhave[*a]

One of the ways of improving the efficiency of polymer solar cell is to increase the conductive paths in the photoactive layer. Present work focuses on the study of effect of additives (Silver nanoparticles (Ag NPs) and Graphene (Gr)) in photoactive Poly 3-hexyl thiophene: Phenyl-C61-butyric acid methyl ester (P3HT:PCBM). The morphology and localised photocurrent obtained using Photon Assisted Conducting Atomic Force Microscopy reflects the role of these additives in the photocurrent produced by the active layer. The study depicts that the morphology of P3HT: PCBM film changes completely with Gr additives, whereas very small change occurs with the addition of Ag NPs. Localised photocurrent masurement exhibits that the space charge limited conduction (SCLC) phenomenon could be the dominant process of charge conduction in P3HT: PCBM film with additives. The study also demonstrats that the carrier mobility enhances by more than an order of magnitude with Gr as additive. This is a significant change for achieving efficient charge separation and transportation in polymer solar cell application.

Introduction

Polymer based photovoltaic cells which are also called organic solar cells has been a field of interest for last several years for their properties such as light weight, flexibility etc [1]. Amongst the materials used for fabricating efficient organic solar cells[2], P3HT:PCBM is the most studied conjugated polymer/fullerene blend [3, 4]. Several studies are under way for enhancing the charge collection efficiency of P3HT: PCBM based solar cells since it is known to be the limiting factor to the efficiency of solar cells based on P3HT: PCBM [5, 6]. Numerous approaches have been reported in this regard such as the use of low band gap polymers [7, 8], different solvents as additives [9, 10], formation of light trapping centres for more absorption using nanostructures [11] and incorporation of metal nanostructures etc. [12, 13]. These additions can result in tailoring the material behaviour in terms of electrical and optical properties [14]. In last few years, various materials such as silver nanostructures, quantum dots, carbon nanostructures etc. have been used in the active layer (of photovoltaic material) to enhance electrical and m optical properties [15-18]. Kim et al. showed the effect of Ag nanowires in active layer in optical and electrical properties. Different aspects have been considered while designing these materials, e.g. to reduce the number of inter particle hopping events to improve the optical absorption in visible region [19].

Department of Applied Physics, Defence Institute of Advanced Technology, Pune-411025, INDIA.
**Corresponding Authors*
[a]*tejashreebhave@diat.ac.in*
[b]*suwarna.datar@gmail.com*

Graphene (Gr) is optically transparent material and has been reported to act as an electron acceptor material in organic solar cells [20]. It has superior electron transport ability and provides high field for better exciton dissociation at the polymer/Gr interfaces as shown by Liu et al. [21, 22]. In polymer solar cells, this type of nanostructure addition helps to provide charge transfer paths which reduce the charge recombination and in turn improve the efficiency of device. When such hetero-structure materials are made, understanding of their charge transfer capability at bulk as well as at nano scale is challenging [23, 24]. It is imperative to study these mechanisms at local interface level. Such study can give better insights into the precise consequences of addition of nanostructures in the polymer.

The solar cell parameters such as short circuit current, open circuit voltage, fill factor etc. provide the information about its performance at macroscopic and device level. These properties are in turn influenced by electron transport within the material at microscopic level. Though these parameters are affected by various processing conditions and blend morphologies, they are insufficient to understand the transport mechanisms at microscopic level [22]. For this, it is very essential to perform localised measurements of photovoltaic material as the basis for further optimisation strategies [25-27].

Conducting atomic force microscopy (C-AFM) is one of the techniques of AFM in which a conducting tip is scanned in contact mode with the sample surface, while a voltage is applied between the tip and the sample [28]. Unlike scanning tunnelling microscopy (STM) and scanning tunnelling spectroscopy (STS) which give information at local level for conducting samples, C-AFM can be used for all types of

materials. It is capable of providing crucial information about the local conducting areas in the sample [29]. As far as the photovoltaic material is concerned this information is extremely useful to characterize the morphology and its correlation with the conducting paths in the photoactive material/layer [30]. It is one of the most promising instruments which can provide abundant information about the morphological behaviour as well electronic properties of the sample [31]. Quantitative information about the resistivity/conductivity at localized level can also be obtained by taking I-V measurements at particular position on the sample [32, 33]. These features have made C-AFM an ideal technique to study electrical transport characteristics in self assembled monolayer, individual molecules and micro fabricated semiconductor devices [34]. Several reports can be found on investigation of electronic properties of metal and semi conductor material through C-AFM [35-38]. Wang et al. have reported conductivity measurement of oxide thin films using C-AFM under UV-light illumination. For the first time, they have directly quantified electron transfer process in hetero-junction semiconductor (WO_3/TiO_2) with the help of photo illumination [39]. Douheret et al. have discussed the ability of C-AFM for conductive polymers like MDMO-PPV:PCBM and demonstrated the donor-acceptor region through spectroscopy [40]. Further, many researchers have rigorously worked on interpretation of C-AFM measurement results, especially calculation on current density and electron mobility using C-AFM [41, 42].

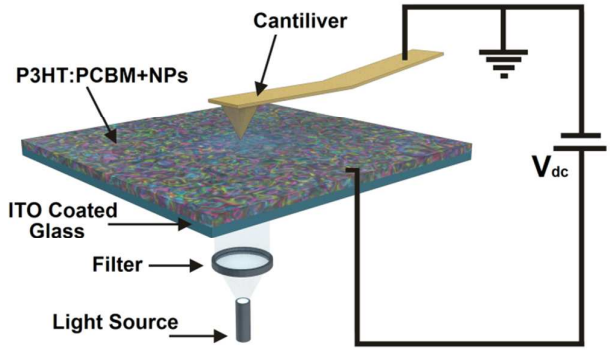

Figure 1: Schematic of an experimental Setup for C-AFM in presence of different band of wavelength (light).

To study similar kind of effects, we have used C-AFM with light illumination (Photon Assisted (PA) C-AFM) as shown in Figure 1. In the present work, Ag NPs and Gr have been used in small percentage as additives in P3HT:PCBM. Three films, P3HT:PCBM, P3HT:PCBM with Ag NPs (P3HT:PCBM_Ag NPs) and P3HT:PCBM with Gr (P3HT:PCBM_Gr) have been studied. This work demonstrates the effect of additives on the charge conduction mechanism of P3HT:PCBM and depicts the effect of additives on the localized photon induced current. In addition to this, calculations have been done to quantify the electron transfer processes in three films.

Experimental

Essential chemicals and substrates for fabrication of photoactive devices were procured from Sigma Aldrich. The surface resistivity of procured ITO (Indium Tin Oxide) coated glass was 8-12 Ω-cm^{-2}. The solution for active layer was prepared with P3HT [Poly 3-hexyl thiophene]:PCBM [phenyl-C_{61}-butyric acid methyl ester] with mass ratio of 1:1 in O-Dichloro benzene (ODCB) [$C_6H_4Cl_2$]. P3HT:PCBM was added in the solvent and was maintained at concentration of 16 mg/ml. The solution was subjected to stirring for a period of 12 hours to mix well before coating on ITO substrate. To study the effect of additive on the transport properties of the photoactive material specifically two additives were tried; Ag NPs and Gr. They were added in weight percentage. Prior to adding Ag NPs and Gr in active material, they were dispersed in ODCB and a solution of 0.05 wt % was prepared. In short, 0.05mg amount of Ag NPs and Gr nanostructures were added in 50 µL solution as an additive for 1 mL photoactive material. The active material was deposited on thoroughly cleaned substrate of ITO coated glass with speed 750 rpm for a period of 60 seconds using Spin coater (spin NXG-P1, Apex). The Active layer was then annealed at a temperature of 120 °C for 20 minutes which was then ready for further characterisation.
The photon absorption by the active material or thin film was observed via UV–Vis spectrophotometer (Specord® 210 plus, Germany). Measurements were done in the visible range i.e. 300 nm to 800 nm. X-ray diffraction (XRD) patterns of the thin films were obtained by a Bruker D8 Advance X-ray diffractometer with grazing incidence geometry. The angle of incidence was positioned to 1° for all samples. Nickel filtered CuKα radiation (α = 1.54 A˚) was used for the scanning angle (2θ) ranging from 2˚ to 50˚ in continuous scan mode with a step size of 0.02°. The surface morphology of the photoactive film was investigated by Field Emission Scanning Electron Microscope (FESEM, ZEISS) at 5 KV. Further, these films were investigated by AFM (Asylum Research) in contact mode in terms of morphological study, electron transport study and optoelectronic study in presence of various ranges of wavelengths. Gold coated silicon nitride AFM tip (radius ~50 nm) was used for entire measurement. Xenon lamp (X-cite, series 120 Q) was used as a light source to illuminate the photoactive material. Three different colours of lights (bands of wavelengths) were used for the study; Violet (330-380 nm), Blue (420-480 nm) and Green (480-550 nm) from dichroic filters provided with the Olympus florescence microscope on which AFM MPF 3D is mounted. All measurements were executed in ambient conditions. Schematic representation of the C-AFM experimental setup is shown in Figure 1.

Results and discussion

UV-Visible Spectroscopy

Presence of P3HT and PCBM in the active layer was confirmed through UV-Vis spectroscopy which is shown in Figure 2. P3HT shows a maximum absorption at 515 nm along with two shoulder peaks at 552 nm and 606 nm, whereas PCBM has a

peak at 336 nm (spectrum (a)). The prominent peak is due to fullerene acceptors in P3HT which enhances the π–π stacking of the polymer chains, and the presence of shoulder peak is due to strong interchain interactions which are responsible for efficient charge transportation and more optical absorption [43]. Ag NPs which are uniformly embedded (see supplementary information (S.I.)) may provide a scattering effect within the polymer matrix. However, there is no significant change observed in absorption after the addition of Ag NPs. This could be due to the phenomenon where the scattered photons may get recaptured by the blend. Spectrum c shows little red shift due to Gr additives. In case of Gr, the red shift might be observed due to increased delocalized excitons in the highly π-conjugated P3HT domains. Delocalized excitons in P3HT:PCBM may increase because of more molecular interaction due to presence of Gr [44, 45]. Since, Gr is sp^2 hybridized material it shows π–π molecular interaction responsible for enhanced delocalisation of excitons. Accordingly, P3HT:PCBM_Gr shows broader range of absorption in visible range as compared to the other two samples. The peak due to the π-π* electronic transitions between 0-1 spin state becomes broader and therefore, more exciton generation is expected subsequent to absorption of photon by photoactive layer [46].

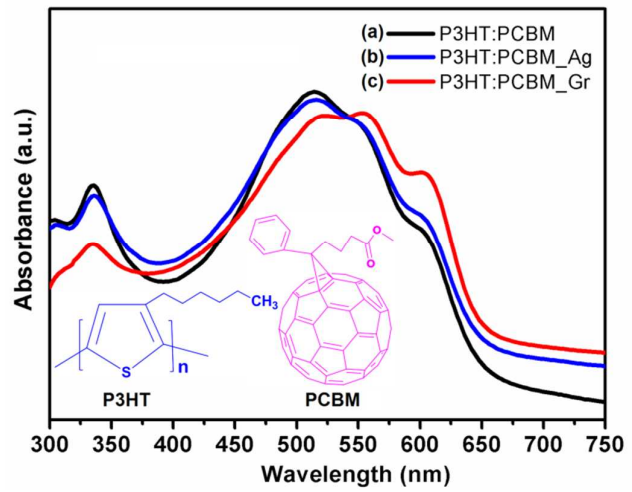

Figure 2: UV-Vis absorption spectra of P3HT:PCBM (a), P3HT:PCBM_Ag NPs (b) and P3HT:PCBM_Gr (c). The inset in figure shows molecular structures of P3HT and PCBM

X-ray Diffraction Analysis

Figure 3 shows the XRD spectra of all the three samples P3HT:PCBM (spectrum (a)), P3HT:PCBM_Ag NPs (spectrum (b)) and P3HT:PCBM_Gr (spectrum (c)). In the spectrum (a) a broad peak at 22° was observed due to PCBM which depicts its amorphous nature, whereas sharp peak was observed at 5.37° (2θ value) due to the reflection plane <100> (edge-on orientation) of thiophene rings in P3HT chain. P3HT has ability to crystallize and has stabilizing effect on the blend morphology [47, 48]. In the blend, crystalline P3HT gets interconnected with the amorphous PCBM. A smaller 'd' spacing for P3HT:PCBM blend may facilitate intermolecular transfer of charge carriers in the film. P3HT:PCBM_Ag NPs showed a strong reflection at 2θ=5.26°, corresponding to an interchain d spacing of 16.8Å. Whereas, P3HT:PCBM_Gr showed interchain d spacing of 16.4Å. This may lead to more intermolecular charge carrier transfer in P3HT:PCBM_Gr layer. The existence of Ag NPs and Gr nanostructures is confirmed by the peaks observed at 38° and 26.5° respectively.

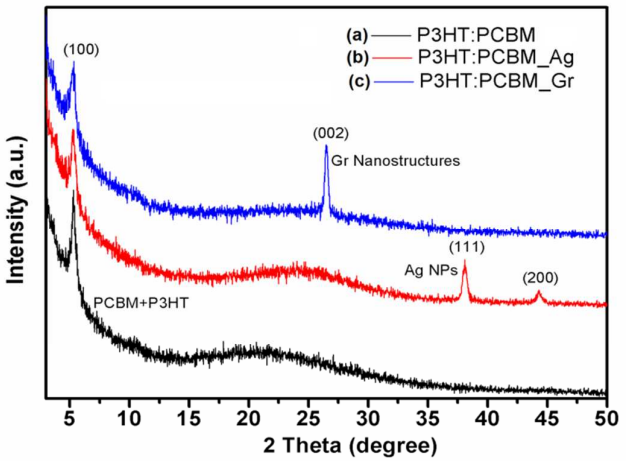

Figure 3: XRD pattern of P3HT:PCBM (a), P3HT:PCBM_Ag NPs (b) and P3HT:PCBM_Gr (c) thin films.

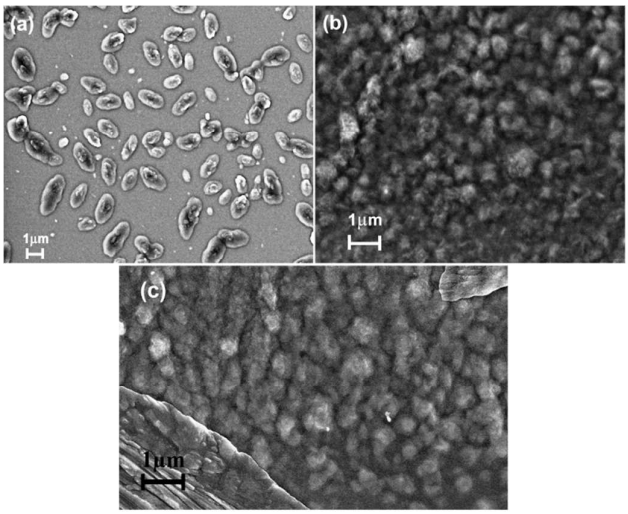

Figure 4: SEM of (a) P3HT:PCBM, (b) P3HT:PCBM_Ag NPs and (c) P3HT:PCBM_Gr thin films.

Field Emission Scanning electron Microscopy

To get the complimentary information about surface morphology, SEM images were obtained as shown in the figure 4. Phase separation of the P3HT and PCBM was observed along with Ag and Gr additives. There was a definite morphological change in terms of phase separation and crystallinity with the additives Ag NPs and Gr in P3HT and PCBM (figure 4 (b) and

(c)). This change definitely would affect the charge transport properties of the films with additives [30, 49]. This was confirmed by C-AFM analysis as discussed in the next section.

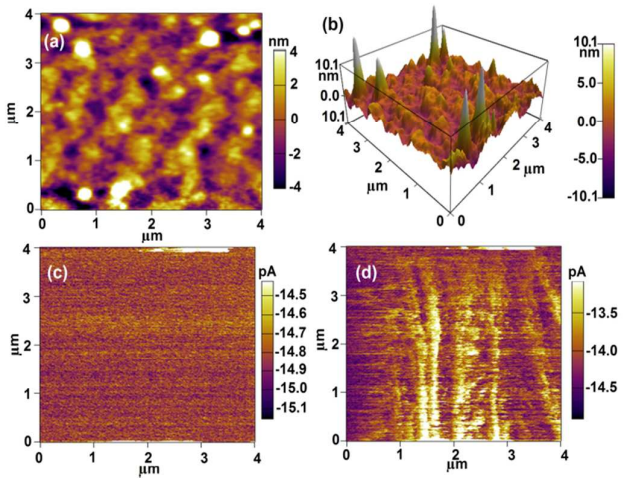

Figure 5: AFM images of P3HT:PCBM shows (a) Morphological view (b) 3–D view (c) current image in no-light (d) current image with exposure of light.

Atomic Force Microscopy Analysis

AFM analysis was performed in two steps. Initially morphology of all the three films was studied. Once a stable image was obtained, current images were recorded from all the samples for applied bias voltages. Figure 5 (a) and (b) shows the morphology and 3-D view of P3HT:PCBM thin film respectively. Figure 5(c) shows its current image under no-light condition. Very less current was observed for the applied bias voltage of 1V for this film. In PA C-AFM studies, films were exposed to different wavelength of bands, i.e. Violet (330-380 nm), Blue (420-480 nm) and Green (480-550 nm). It was found that exposure to different wavelengths showed current from various regions. The result under the light exposure is shown in Figure 5 (d).

Similar experiments were performed on P3HT:PCBM_Ag NPs and P3HT:PCBM_Gr and the results are shown in Figure 6 and Figure 7 respectively. There was no substantial change in the morphology due to the applied bias or exposure of light in these films (see supplementary information (S.I.)). We could observe increase in the localized current in P3HT:PCBM_Ag NPs as compared to P3HT:PCBM (Figure 6 (c)) although the current distribution in the film was not uniform. In fact, there was not much quantitative change in the current image of P3HT:PCBM_Ag NPs as we exposed the films to different wavelength ranges as compare to P3HT:PCBM (see S.I.). As discussed in the previous section Ag NPs act as scattering centers and this could be one of the reasons why we could not observe much change in the PA C-AFM data for this sample. But interestingly the current was observed from different regions for light exposure (Figure 6 (d)). On the other hand one could see the morphology of the film completely changed in P3HT:PCBM_Gr (Figure 7 (a)). Since the surface area of Gr is

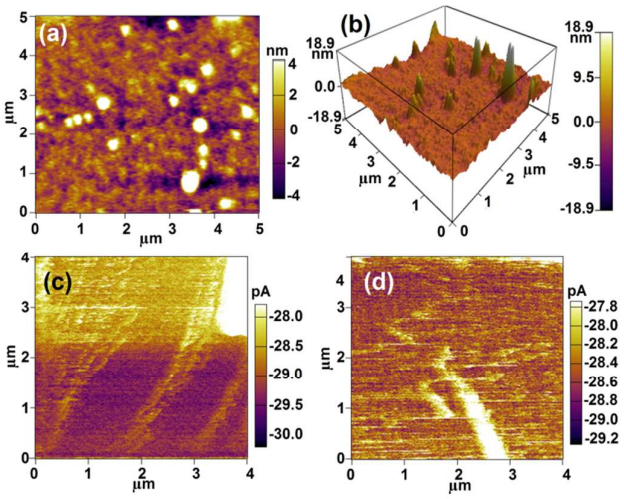

Figure 6: AFM images of P3HT:PCBM_Ag NPs shows (a) Morphological view (b) 3–D view (c) current image in no-light (d) current image with exposure of light.

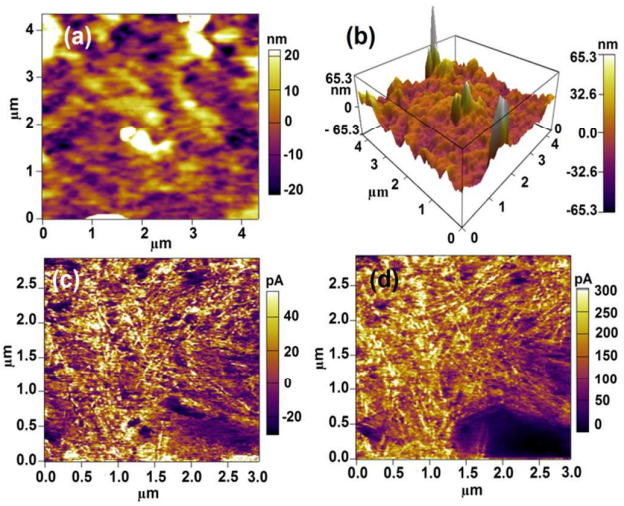

Figure 7: AFM images of P3HT:PCBM_Gr shows (a) Morphological view (b) 3–D view (c) current image in no-light (d) current image with exposure of light.

very large [18, 50], its dispersion in the film alters the morphology drastically compared to Ag NPs. The observation was also supported by the current images obtained from the films. One could see the current from almost the entire scanned area of P3HT:PCBM_Gr under no-light condition (Figure 7 (c)). Also, as shown in Figure 6 (d) the current from the film changes by an order of magnitude when exposed to light. The image shown in the figure exhibits the exposure of green light (480-550nm) for which the current was maximum. The AFM images for all the samples were taken at constant load on the tip to ensure that the changes in the I-V measurements for different samples were predominantly due to the changes in the sample resistivity. The current increased by an order of magnitude with the addition of Gr and in presence of green light (480-550 nm).

To further understand the conductivity mechanism in the films, I-V measurements were made using C-AFM with gold coated silicon nitride cantilever for no-light and in presence of light of different bands of wavelength for all the samples. I-V measurements were taken at around 10 different locations in each film. At each location the data was recorded at least 10 times to confirm the repeatability of the measurements. The data shown in the figure depicts the averaged out data with the variation of ±5%. Averaged I-V plots for the comparison in no-light condition for all the films are shown in Figure 8 (a). A very small current was observed for the P3HT:PCBM for large bias range of -7 to +7 V. This was consistent with current images obtained, as there was no current observed for this sample under no-light condition. The current increased slightly for P3HT:PCBM_Ag NPs and there was a significant increment in the current for P3HT:PCBM_Gr. The inset shown in Figure 8 (a) compares the current variation between P3HT:PCBM and P3HT:PCBM_Ag NPs, since in Figure 8 (a) variation between these cannot be clearly distinguished. Figure 8 (b), (c) and (d) show the effect of light on all the three samples. One can see

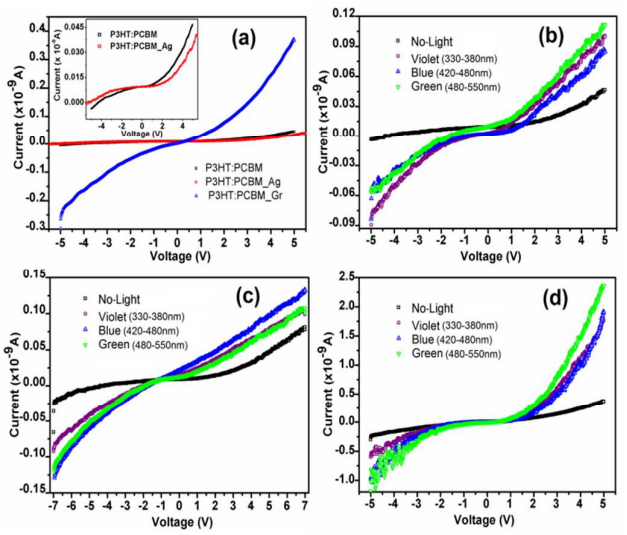

Figure 8: Current–voltage analysis of (a) P3HT:PCBM, P3HT:PCBM_Ag NPs and P3HT:PCBM_Gr in no-light. Inset figure shows comparison between P3HT:PCBM and P3HT:PCBM_Ag NPs. (b) P3HT:PCBM in No-Light, Violet (330-380 nm), Blue (420-480 nm) and Green (480-550 nm) (c) P3HT:PCBM_Ag NPs in No-Light, Violet (330-380 nm), Blue (420-480 nm) and Green (480-550 nm) (d) P3HT:PCBM_Gr in No-Light, Violet (330-380 nm), Blue (420-480 nm) and Green (480-550 nm).

that the current has increased in all the samples upon exposure of violet (330-380 nm), blue (420-480 nm) and green (480-550 nm). The experiments were performed several times and in both the directions i.e. from no-light to light and vice versa to ensure the consistency of the results. The changes in the electronic band gap of the photoactive material with additives (Ag NPs and Gr) and exposure of light was observed clearly. The results have been tabulated (table 1) related to (a) optical band gap using UV-Vis spectroscopy and (b) electronic band gap using C-AFM data. From table 1, one can notice that, calculated optical band gap are almost similar as electronic band gap of respective photo active materials. In P3HT:PCBM_Ag NPs there was change in the shape of the I-V curve after exposure to light while the current still remained comparable to the P3HT:PCBM. Also, there was no systematic response observed for exposure of light. On the other hand, in case of P3HT:PCBM_Gr, there was an order of magnitude increase in the current when it was exposed to different wavelengths of light. In these films maximum current was observed for the exposure of green light (480-550 nm) (Figure 8d). The results are consistent with the C-AFM results though they cannot be compared quantitatively. This may be due to the two possible reasons; (1) the distance between AFM tip and sample changes during the I-V measurement and (2) the current obtained through the scanning is an average current from 4x4 µm areas, whereas in the I-V measurement, particular spot may give a higher current than the entire area under the exposure of different wavelength of light.

Table 1:- Band gap of photoactive material calculated (a) Optical band gap using UV-Vis spectroscopy (Tauc plot) and (b) electronic band gap using C-AFM data.

Sr. No.	Sample	λ_{max} (nm)	E_g (eV) (optical)	E_g (eV) (electronic)
1	P3HT:PCBM	516	2.41	2.50
2	P3HT:PCBM_Ag	521	2.38	2.29
3	P3HT:PCBM_Gr	556	2.23	2.16

Space Charge Limited Conduction (SCLC)

The performance of the active layer depends on the rate at which the charged carriers get separated and transported to the respective electrodes which helps in avoiding further recombination. This can be achieved by making pathways available in the film for the charge transfer [51]. Charge transfer in bulk hetero junctions is a complicated process. The I-V measurements carried out by C-AFM can throw some light on the understanding of the charge transfer mechanism in the present scenario. Mainly, there are two types of conduction mechanisms which can be considered, one in which the conduction is dominated by the contact between the electrode and the material (electrode limited conduction) and another in which the conduction is primarily due to properties of the material (bulk limited). Most of the times, the I-V measurements constitute combination of more than one type of conduction mechanism. Therefore, it is difficult to pinpoint one particular mechanism responsible for conduction. Electrode limited processes such as Schottky process is a temperature dependent phenomenon, whereas Fowler-Nordheim (F-N) is a tunnelling phenomenon. In both these cases barrier height plays an important role. In the measurements done in C-AFM in contact mode, though these processes cannot be completely ruled out, bulk limited conduction mechanisms were considered more suitable in the present study of the films. The bulk limited conduction depends on the properties of the materials under consideration. In this Poole-Frankel (P-F) mechanism does not come in picture since it dominates primarily at higher temperatures. A log-log plot of current density-voltage (J-V)

characteristics shows the typical regions of SCLC. The log-log curve of J-V for space charge limited current has three regions; (i) Ohm's law where current is linearly proportional to the field, (ii) trap-filled limited (TFL) conduction & (iii) Child's law where current is proportional to the square of the field. The expressions for current density in these regions are represented as equation 1, 2 and 3 respectively [52-54]

$$J_{Ohm} = qn_0\mu\frac{V}{d} \quad (1)$$

$$J_{TFL} = \frac{9}{8}\mu\varepsilon\theta\frac{V^2}{d^3} \quad (2)$$

$$J_{Childs} = \frac{9}{8}\mu\varepsilon\frac{V^2}{d^3} \quad (3)$$

where q is electronic charge, n_o is concentration of free charge carriers, μ is the electronic mobility, ε is dielectric constant, θ is the ratio of free carrier density to total carrier density, V is applied voltage and d is thickness of the sample.

In such measurements done using C-AFM, various aspects and parameters come into consideration e.g. type of tip material, diameter, force, geometry configuration etc. and hence it limits the different conduction mechanisms including SCLC [55, 56]. Many research groups [30, 41] have put their efforts to investigate and extract a new scaling relationship for accurate interpretation of the samples. Following the in-depth analysis, Mott-Gurney law turns into new form which is shown in equation 4.

$$J = \propto \varepsilon\varepsilon_o\mu e^{0.89\gamma\sqrt{V/L}}\ \frac{V^2}{L^3}\delta\left(\frac{L}{d}\right)^{1.6\pm0.1} \quad (4)$$

Here α is 8.2 (in place of 9/8 in eq. (2)), ε_o is permittivity in free space, γ is field dependence mobility enhancement factor (for P3HT=0), δ is scaling factor, L is thickness of the film and d is the diameter of AFM tip.

Figure 9 (a) shows the comparison of log-log plots of J-V measurement of P3HT:PCBM, P3HT:PCBM_Ag and P3HT:PCBM_Gr under no-light conditions. The plots for P3HT:PCBM and P3HT:PCBM_Ag clearly show three different regions; ohms law region, trap-filled-limited region, and Child's law region. At low applied voltage where the curve shows ohmic behaviour, the density of thermally generated charged carriers is supposed to be higher than the injected charges. Above a particular voltage V_{ON} (0.72 V in the case of P3HT:PCBM) injected carriers dominate and fill the traps until the voltage V_{TFL} is reached (2.41V). Above this voltage and at higher injection rate all traps are filled and conduction becomes space charge limited (Child's law). Beyond V_{TFL}, all the current is due to space charge. Comparable voltages for V_{ON} and V_{TFL} were also seen for P3HT:PCBM_Ag NPs (table 2). Interestingly, one can see that there is less effect of Ag NPs as far as the conduction mechanism is concerned. However, for P3HT:PCBM_Gr the V_{ON} (0.15V) goes down (the onset of the SCLC decreases) along with decrease in the V_{TFL} (0.66V). Thus, with Gr, Child's law is the dominant conduction mechanism. Similar effects were observed, when the films were exposed to light. Based on the SCLC; V_{ON}, V_{TFL}, and mobility (μ) of the charged carriers were found out. These values are tabulated (table 2) for different samples and the exposure to different wavelengths (lights). The carrier mobility in P3HT:PCBM_Ag NPs film remains comparable to P3HT:PCMB film while it changes (from $3x10^{-7}$ to $74.6x10^{-6}$ m^2/vs) by two orders of magnitude in P3HT:PCBM_Gr film. This carrier mobility was calculated with the help of equation 2. To take into consideration the geometry of the C-AFM system carrier mobility was also determined using equation 4. It was observed that, after considering the effect of d and γ, carrier mobility changes by an order which is shown in table 3. Mobility change due to Gr is significant in order to achieve efficient charge separation and transportation.

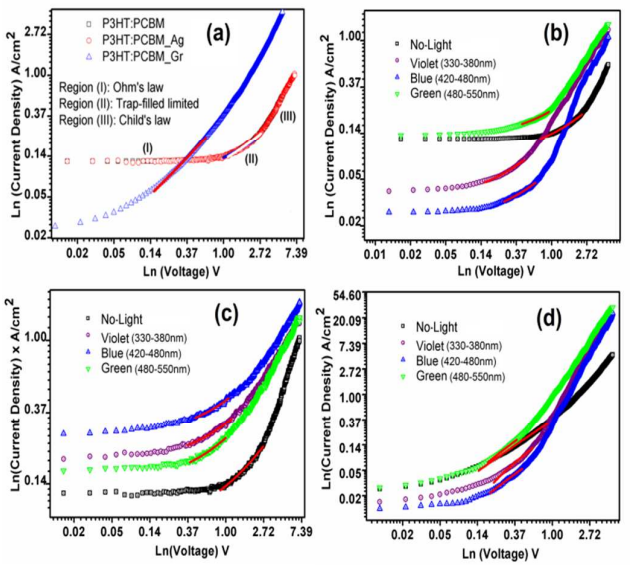

Figure 9: Log-log plot of J vs V (a) P3HT:PCBM, P3HT:PCBM_Ag and P3HT:PCBM_Gr in No-Light (b) P3HT:PCBM in No-Light, Violet (330-380 nm), Blue (420-480 nm) and Green (480-550 nm)s (c) P3HT:PCBM_Ag NPs in No-Light, Violet (330-380 nm), Blue (420-480 nm) and Green (480-550 nm) (d) P3HT:PCBM_Gr in No-Light, Violet (330-380 nm), Blue (420-480 nm) and Green (480-550 nm).

Table 2: Electrical parameter of P3HT:PCBM, P3HT:PCBM_Ag NPs and P3HT:PCBM_Gr for different exposure of band of wavelengths which is calculated by equation 2.

Sr. No.	Band Of Wavelength (nm)	P3HT:PCBM			P3HT:PCBM_Ag			P3HT:PCBM_Gr		
		V_{ON} (V)	V_{TFL} (V)	μ m^2/Vs	V_{ON} (V)	V_{TFL} (V)	μ m^2/Vs	V_{ON} (V)	V_{TFL} (V)	μ m^2/Vs
1	No Light	0.72	2.41	$3x10^{-7}$	0.86	2.37	$26.3x10^{-6}$	0.15	0.66	$74.6x10^{-6}$
2	Violet (330-380)	0.14	0.46		0.36	1.19		0.21	0.60	
3	Blue (420-480)	0.25	0.63		0.43	1.1		0.18	0.45	
4	Green (480-550)	0.42	0.94		0.40	1.0		0.18	0.39	

Table 3: Carrier mobility of P3HT:PCBM, P3HT:PCBM_Ag NPs and P3HT:PCBM_Gr calculated by different equations(Eqn.2 and Eqn.4)

Sr. No.	Sample	μ (m^2/Vs) through Eq. (2)	μ (m^2/Vs) through Eq. (4)
1	P3HT_PCBM	3×10^{-7}	4.62×10^{-5}
2	P3HT_PCBM_Ag	26.3×10^{-6}	6.65×10^{-5}
3	P3HT_PCBM_Gr	74.6×10^{-6}	1.88×10^{-4}

Conclusions

In the current work we have discussed the effect of Ag NPs and Gr additives on the conduction mechanism of photoactive material P3HT:PCBM using C-AFM and PA C-AFM. It was observed that Ag and Gr additives provided different conductive paths in presence of different band of wavelength the films were exposed to. It was also observed that compared to Ag, presence of Gr in P3HT:PCBM enhanced the light trapping capability of the film. This reflected in enhanced current in C-AFM in Gr compared to other two samples. In addition, Gr turned out to be the most promising additive as it provided conducting paths throughout the scanned sample area. In the transport study, child's law dominated conduction mechanism was observed in P3HT:PCBM_Gr films. The carrier mobility in P3HT:PCBM_Gr increased by an order of magnitude compared to P3HT:PCBM. With these studies, it has been demonstrated that C-AFM and PA C-AFM can provide unique insight in the current conduction mechanisms in the photoactive materials.

Acknowledgements

Mr. Pramod Bankar is acknowledged for AFM measurements. Sanjay Sahare, Suwarna Datar and Tejashree Bhave would like to acknowledge financial assistance from ERIP/ER/1003883/M/01/908/2012/D(R&D)/1416 project.

Reference

1 J. You, L. Dou, Z. Hong, G. Li, and Y. Yang, *Prog. Polym. Sci*., 2013, **38**, 1909.
2 S. B. Darling and F. You, *RSC Adv*., 2013, **3**, 17633.
3 A. M. Ballantyne, T. A. M. Ferenczi, M. Campoy-Quiles, T. M. Clarke, A. Maurano, K. H. Wong, W. Zhang, N. Stingelin-Stutzmann, J. S. Kim, D. D. C. Bradley, J. R. Durrant, I. McCulloch, M. Heeney, J. Nelson, S. Tierney, W. Duffy, C. Mueller and P. Smith, *Macromolecules,* 2010, **43**, 1169.
4 F. Jin, B. Chu, W. Li, Z. Su, X. Yan, J. Wang, R. Li, B. Zhao, T. Zhang, Y. Gao, C.S. Lee, H. Wua, F. Hou, T. Lin, and Q. Song, *Org. Electron.,* 2014, **15**, 3756.
5 M. Glatthaara, M. Riede, N. Keegan, K. Sylvester-Hvid, B. Zimmermann, M. Niggemann, A. Hinsch and A. Gombert, *Sol. Energy Mater. Sol. Cells,* 2007, **91,** 390.
6 R. A. J. Janssen and J. Nelson, *Adv. Mater.* 2013, **25**, 1847.
7 E. Bundgaard, and F. C. Krebs, *Sol. Energy Mater. Sol. Cells,* 2007, **91**, 954.
8 L. Lu and L. Yu, *Adv. Mater.,* 2014, **26**, 4413.
9 T. Xu and L. Yu, *Materials Today,* 2014, **17**, 11.
10 X. Guo, N. Zhou, S. J. Lou, J. Smith, D. B. Tice, J. W. Hennek, R. P. Ortiz, J. T. Lopez Navarrete, S. Li, J. Strzalka, L. X. Chen, R. P. H. Chang, A. Facchetti, and T. J. Marks, *Nat. Photon.,* 2013, **7**, 825.
11 R. Po, C. Carbonera, A. Bernardi, and N. Camaioni, *Energy Environ. Sci.*, 2011, **4**, 285.
12 H. Chen and L. Wang, *Beilstein J. Nanotechnol.* 2014, **5**, 696.
13 S. Linic, P. Christopher and D. B. Ingram, *Nature Materials*, 2011, **10**, 911.
14 I. Gur, N. A. Fromer, M. L. Geier, A. P. Alivisatos, Science 310, 462 (2005).
15 W. J. E. Beek, M. M. Wienk, and R. A. J. Janssen, *Adv. Funct. Mater.*, 2006, **16**, 1112.
16 E. Singh and H. S. Nalwa, *RSC Adv.* 2015, **5**, 73575.
17 J. A. Andre´s, and W. J. Blau, *Carbon*, 2008, **46**, 2067.
18 C. T. Chien, P. Hiralal, D. Y. Wang, I. S. Huang, C. C. Chen, C. W. Chen, and G. A. J. Amaratunga, *Small*, 2015, **11**, 2929.
19 C. H. Kim, S. H. Cha, S. C. Kim, M. K. Song, J. Lee, W. S. Shin, S. J. Moon, J. H. Bahng, N. A. Kotov, and S. H. Jin, *ACS Nano* 2011, **5**, 3319.
20 W. R. Lian, Y. C. Huang, Y. A. Liao, K. L. Wang, L. J. Li, C. Y. Su, D. J. Liaw, K. R. Lee, and J. Y. Lai, *Macromolecules*, 2011, **44**, 9550.
21 Z. Liu, D. He, Y. Wang, H. P. Wu, and J. Wang, *Synthetic Metals*, 2010, **160**, 1036.
22 G. H. Jun, S. H. Jin, B. Lee, B. H. Kim, W. S. Chae, S. H. Hong, and S. Jeon, *Energy Environ. Sci.*, 2013, **6**, 3000.
23 C. Hamann, H. Burghardt and T. Fraunheim, Electrical conduction mechanism in solids, VEB Deutsher Verlag der Wisenschaften, Berlin, Germany 1988.
24 W. Yang, Y. Yao, and C.Q. Wu, Org. Electron. 2013, 14, 1992.
25 C.I. Zanetti, A. Mechler, S.A. Carter, and R. Lal, Adv. Mater. 2004, 16, 385.
26 J.A. Stroscio, R.M. Feenstra, and A.P. Fein, Phys. Rev. Lett. 1986, 57, 2579.
27 Y. Liang, D. Feng, Y. Wu, S.T. Tsai, G. Li, C. Ray, and L. Yu, J. *Am. Chem. Soc*., 2009, **131**, 7792.
28 G. Binnig, C.F. Quate, and C. Gerber, *Phys. Rev. Lett.,* 1986, **56**, 930.
29 D. Moerman, N. Sebaihi, S. E. Kaviyil, P. Leclere, R. Lazzaroni, O. Douheret, *Nanoscale*, 2014, **6**, 10596.
30 K. Maturova, S. S. Van Bavel, M. M. Wienk, R. A. J. Janssen M. Kemerink, *Nano Lett.* 2009, **9**, 3032.
31 J. Planes, F. Houze, P. Chretien, and O. Schneegans, *Appl. Phy. Lett.,* 2001, **79**, 2993.
32 V. B. Engelkes, J. M. Beebe, and C. D. Frisbie, *J. Phys. Chem. B,* 2005, **109**, 16801.
33 S. Desbief, N. Hergue, O. Douheret, M. Surin, P. Dubois, Y. Geerts, R. Lazzaroni, P. Leclere, *Nanoscale*, 2012, **4**, 2705.
34 N. J. Tao, *Nat. Nanotech.,* 2006, **1**, 173.
35 T. W. Kelley, E. L. Granstrom, and C. D. Frisbie, *Adv. Mater.,* 1999, **11**, 261.
36 C. J. Boxley, H. S. White, C. E. Gardner, and J. V. Macpherson, *J. Phys. Chem. B,* 2003, **107**, 9677.
37 H. N. Lin, H. L. Lin, S. H. Chen, L. S. Yu, G. Y. Perng, S. A. Chen, and S. H. Chen, *Appl. Phys. Lett.*, 2002, **81**, 2572.
38 J. Alvarez, I. Ngo, M. E. Gueunier-Farret, J. P. Kleider, L. Yu, P. R. Cabarrocas, S. Perraud, E. Rouviere, C. Celle, C. Mouchet, and J. P. Simonato, *Nanoscale Research Letters,* 2011, **110**, 1.
39 S. Wang, X. Zhang, G. Cheng, X. Jiang, Y. Li, Y. Huang, and Z. Du, Chem. Phys. Lett. 2005, 405, 63.
40 O. Douheret, L. Lutsen, A. Swinnen, M. Breselge, K. Vandewal, L. Goris, and J. Manca, *Appl. Phys. Lett.*, 2006, **89**, 032107.
41 O. G. Reid, K. Munechika, D. S. Ginger, *Nano Lett.*, 2008, **8**, 1602.
42 D. S. Coffey, O. G. Reid, D. B. Rodovsky, G. P. Bartholomew, D. S. Ginger, *Nano. Lett.*, 2007, **7**, 738.
43 L. Ye, S. Zhang, D. Qian, Q. Wang, and J. Hou, *J. Phys. Chem. C,* 2013, **117**, 25360.
44 Y. Ren, A. K. Hailey, A. M. Hiszpanski, and Y. L. Loo, *Chem. Mater.*, 2014, **26**, 6570.

45 J. T. Bloking, X. Han, A. T. Higgs, J. P. Kastrop, L. Pandey, J. E. Norton, C. Risko, C. E. Chen, J. L. Bredas, M. D. McGehee, and A. Sellinger, *Chem. Mater.*, 2011, **23**, 5484.
46 P. P. Khlyabich, B. Burkhart, A. E. Rudenko, and B. C. Thompson, *Polymer*, 2013, **54**, 5267.
47 U. Zhokhavets, T. Erb, G. Gobsch, M. Al-Ibrahim, and O. Ambacher, *Chem. Phys. Lett.*, 2006, **418**, 347.
48 Y. H. Chen, P. T. Huang, K. C. Lin, Y. J. Huang, and C. T. Chen, *Org. Electron.*, 2012, **13**, 283.
49 T. Erb, U. Zokhavets, G. Gobsch, S. Releva, B. Stuhn, P. Schilinsky, C. Waldauf, C. J. Brabec, *Adv. Funct. Mater.*, 2005, **15**, 1193.
50 Z. Li, B. Song, Z. Wu, Z. Lin, Y. Yao, K. S. Moon, and C. P. Wong, *Nano Energy*, 2015, **11**, 711.
51 S. W. Heo, K. H. Baek, H. J. Song, T. H. Lee, and D. K. Moon, *Macromol. Mater. Eng.*, 2014, **299**, 353.
52 F. C. Chiu, H. W. Chou, and J. Y. Lee, *J. Appl. Phys.,* 2005, **97**, 103503.
53 M. Stadele, F. Sacconi, A. Di Carlo, and P. Lugli, *J. Appl. Phys.*, 2003, **93**, 2681.
54 B. Brar, G. D. Wilk, and A. C. Seabaugh, *Appl. Phys. Lett.*, 1995, **67**, 1031.
55 P. Atten, K. Adamiak, B. Khaddour and J. L. Coulomb, *J. Optoelectron. Adv. Mater.*, 2004, **6**, 1023.
56 A. A. Grinberg, S. Luryi, M. R. Pinto and N. L. Schryer, *IEEE Trans. Electron Devices*, 1989, **36**, 1162.

Photon assisted conducting atomic force microscopy study of nanostructured additives in P3HT:PCBM

Sanjay Sahare, Naresh Veldurthi, Suwarna Datar[*b] and Tejashree Bhave[*a]

Department of Applied Physics, Defence Institute of Advanced Technology, Pune-411025, INDIA.

**Corresponding Authors: [a]tejashreebhave@diat.ac.in; [b]suwarna.datar@gmail.com*

Tel: +91 20 2430 4093; Fax: +91 20 2438 9411

Graphical Abstract

P3HT:PCBM demonstrates the enhanced current with additives like Ag NPs and Gr nanoflexes. The continuous conducting paths attributes the Gr nanoflexes with an order of higher magnitude than Ag NPs. The results have been consistent under various photon wavelength exposures, studied under the Photon assisted conducting microscopy.